The peak absorbance wavelength of photosynthetic pigments around other stars from spectral optimization

Owen R. Lehmer, David C. Catling, Mary N. Parenteau, Nancy Y. Kiang, and Tori M. Hoehler

June 16, 2021

Abstract

In the search for life on other planets, the presence of photosynthetic surface vegetation may be detectable from the colors of light it reflects, which on the modern Earth is a steep increase in reflectance between the red and near-infrared wavelengths, a "red edge." This edge-like signature occurs at wavelengths of peak photon absorbance, which are the result of adaptations of the phototroph to their spectral environment. On planets orbiting different stellar types, red edge analogs may occur at other colors than red. Thus, knowing the wavelengths at which photosynthetic organisms preferentially absorb and reflect photons is necessary to detect red edge analogs on other planets. Using a numerical model that predicts the absorbance spectrum of extant photosynthetic pigments on Earth from Marosvölgyi & van Gorkom (2010), we calculate the absorbance spectrum for pigments on an Earth-like planet around F through late M type stars that are adapted for maximal energy production. In this model, cellular energy production is maximized when pigments are tuned to absorb at the wavelength that maximizes energy input from incident photons while minimizing energy losses due to thermal emission and building cellular photosynthetic apparatus. We find that peak photon absorption for photosynthetic organisms around F type stars tends to be in the blue while for G, K, and early M type stars, red or just beyond is preferred. Around the coolest M type stars, these organisms may preferentially absorb in the near-infrared, possibly past 1 micron. These predictions are consistent with previous, qualitative estimates of pigment absorptance. Our predicted absorbance spectra for photosynthetic surface organisms depend on both the stellar type and planetary atmospheric composition, especially atmospheric water vapor concentrations, which alter the availability of surface photons and thus the predicted pigment absorption. By constraining the absorbance spectra of alien, photosynthetic organisms, future observations may be better equipped to detect the weak spectral signal of red edge analogs.

1 Introduction

Oxygenic photosynthetic organisms dominate primary productivity on the modern Earth (e.g. Field et al., 1998). Abundant, green surface vegetation is a prominent example of such productivity. While surface vegetation slightly reflects green photons in the visible spectrum, the strongest spectral reflectance occurs just beyond the visible in near-infrared (NIR) wavelengths. This sharp contrast in absorbance in the red and reflectance in the NIR is termed the "vegetation red edge" or simply the "red edge." This spectral signature is sufficiently strong on the modern Earth and distinct from mineral spectra that satellite observations of it are used to map the presence and activity of vegetation (Tucker & Maxwell, 1976). It thus serves as a model for similar reflectance biosignatures that future telescope observations could detect on an Earth-like exoplanet (e.g. Sagan et al., 1993; Seager et al., 2005; Kiang et al., 2007b; O'Malley-James & Kaltenegger, 2018; Wang & He, 2021).

The absorption of red photons by green land plants is due to chlorophyll *a* (Chl *a*), which is the primary photopigment in oxygen-producing photosynthetic organisms, such as algae and cyanobacteria on the modern Earth. In these organisms, Chl *a* and other light harvesting pigments absorb photons across the visible, with the long wavelength cut-off where Chl *a* absorbs red photons, peaking at 680 and 700 nm. In plant leaves, strong scattering occurs in the NIR due to the change in the index of refraction between leaf mesophyll cell walls and air spaces in the leaf and lack of absorbance by pigments (Gausman, 1974). This step-like change in spectral absorbance results in the red edge.

In all phototrophs, accessory pigments often accompany the primary photopigment, providing additional photon harvesting. Photon absorption for Chl *a* peaks in the blue and red, and accessory pigments offer additional spectral coverage. The excitation energy of shorter wavelength, higher-energy photons is stepped down through energetically favorable resonant transfer to the red absorbance of Chl *a*, which trap that energy in a reaction center (e.g. Blankenship, 2008). The excess photon energy is released as heat during this transfer process so that each photon absorbed by the photosynthetic cell provides an input energy to Chl *a* equivalent to a red photon. The reaction center Chl *a* molecules enable charge separation; that is, the excited pigment provides the conversion of photon energy to chemical potential, giving up an excited electron for electron transfers in biochemical reactions. Around other stars, Chl *a* analogs could arise in the form of different pigments that may be tuned to absorb photons at different wavelengths, changing the wavelength of a vegetative red edge analog. See Schwieterman et al. (2018) and Blankenship (2008, 2014) for thorough discussions of Chl *a* and the molecular mechanisms of photosynthesis.

The structure of Chl *a* has been attributed to evolution from simpler porphyrins, or the chemical properties required of a pigment to participate in oxygenic photosynthesis (e.g. Mauzerall et al., 1976; Björn et al., 2009; Björn & Ghiradella, 2015). In addition, optimization arguments based on the available radiation spectrum have been proposed as a driver for the structure and absorbance spectrum of Chl *a* (Björn, 1976;

Stomp et al., 2007; Kiang et al., 2007a; Milo, 2009; Marosvölgyi & van Gorkom, 2010; Ritchie et al., 2017; Arp et al., 2020). Kiang et al. (2007b), Stomp et al. (2007), and Ritchie et al. (2017) observed that the absorption wavelength for reaction center pigments in extant organisms correlates with spectral peaks in the incident photon flux per uniform wavelength interval. However, Björn (1976) and Milo (2009) noted that such correlations may be somewhat artificial, as the wavelength of peak photon flux depends on whether one considers photons per uniform frequency interval, or photons per uniform wavelength interval. Therefore, optimality arguments based on maximal rates of energy storage have been explored (Björn, 1976; Milo, 2009; Marosvölgyi & van Gorkom, 2010).

Björn (1976) considered how incident flux constrains the maximum achievable chemical potential in optically thin systems, such as in unicellular photosynthetic organisms. By approximating the Sun as a blackbody and accounting for thermal emission of pigments, Björn (1976) showed that, in full sunlight, chemical energy production is maximized in photosynthetic surface organisms when absorbing near 700 nm. A similar optimal wavelength was found by Milo (2009) by considering the energetic overhead encountered during photosynthesis to move electrons from H_2O to NADPH, termed an "overpotential." Using the empirical overpotential of Photosystems I and II along with the spectrally resolved flux available at the Earth's surface, Milo (2009) found pigment absorption was optimized between 680 and 720 nm. Marosvölgyi & van Gorkom (2010) extended the work of Björn (1976) to consider optically thick systems, accounting for the possibility of multiple dipoles, and the spectrally resolved incident Solar flux considered by Milo (2009). In addition, Marosvölgyi & van Gorkom (2010) considered the energetic cost for a cell to create pigments and store photosynthetic energy, an important consideration raised by Milo (2009). With these enhancements to the model of Björn (1976), Marosvölgyi & van Gorkom (2010) showed that Chl a is optimized when peak absorption occurs at ~ 680 nm, the Q_y band of *in vivo* Chl a, and that the measured absorption profile of Chl a around that peak is similarly optimal. In addition, substituting the surface photon flux for the ambient photon flux in the water column, Marosvölgyi & van Gorkom (2010) found that the same pigment optimization model reproduced the absorbance profile of *Rhodobacter sphaeroides* chromatophores in the NIR.

While Marosvölgyi & van Gorkom (2010) optimized power gain based on incident flux to predict pigment absorbance spectra, Arp et al. (2020) assumed a fixed power demand by photosynthetic organisms to determine the optimal wavelength for pigment absorption. Arp et al. (2020) examined the role of antenna light harvesting pigments in picking out separate spectral bands of an organism's light environment to minimize the mismatch between the energy supply and demand. A two-absorber system at separate bands helps to ensure a steadier power supply, which can be generalized to more absorbers. This scheme appears to predict wavelengths of peak absorbance for both the trap and Soret band wavelengths for Chl a-bearing organisms, but the role of light quality for underwater and anoxygenic phototrophs is less clear. Because this scheme does not directly model the actual light harvesting processes and requires

assumptions of the shape of the pigment absorbance peaks and the number of absorbers, we adopt the model of Marosvölgyi & van Gorkom (2010) to be agnostic to these specifications and to more directly simulate light energy use processes in this work. The model of Marosvölgyi & van Gorkom (2010) requires only the available photon flux to predict plausible pigment absorbance spectra, thus it could constrain the absorbance spectra of surface pigments around other stars.

Prediction of pigment absorption around other stars has been considered previously, but via a simplified model with stars approximated as blackbodies (Lehmer et al., 2018), or qualitatively based on the incident spectral flux (Kiang et al., 2007b; Ritchie et al., 2017; Takizawa et al., 2017). Based on the observed correlations between photon flux and pigment peak absorbance wavelengths, Tinetti et al. (2006) proposed a red edge analog for an M dwarf star could be near 1.1 μm. Takizawa et al. (2017) also explored photosynthesis around M dwarf stars, but considered how multi-band photosystems might be restricted in different spectral light environments and did not attempt to predict light harvesting pigment spectra precisely.

Here, we apply the power gain optimization model of Marosvölgyi & van Gorkom (2010) to the Earth around other stars to predict the absorbance spectra of alien photoautotrophs. Using simulated surface spectra through the modern Earth's atmosphere for F2V through M5V stars from Kiang et al. (2007b), we predict the absorption peak and profile of pigments for various stellar types. Our predictions could inform future observations looking for the photosynthetic red edge as a possible biosignature (Sagan et al., 1993; Seager et al., 2005; Kiang et al., 2007b; O'Malley-James & Kaltenegger, 2018; Wang & He, 2021) and provide a quantitative update to the qualitative predictions for red edge analogs around other stars from Kiang et al. (2007b).

2 Methods

To predict optimal pigment absorption based on incident photon flux, we use the model initially developed by Björn (1976) then refined and justified in detail by Marosvölgyi & van Gorkom (2010). Our implementation recreates the numerical model described in Marosvölgyi & van Gorkom (2010), which we summarize below.

The model solves for an absorbance spectrum that optimizes power gain in an optically thick suspension of photosynthetic cells. It does so by considering the incident flux available for absorption, thermal emission, and the costs to build the photosynthetic apparatus. With incident flux known, the input energy intensity over all frequencies in W m^{-2}, P_{in}, is given by

$$P_{in} = J_L \cdot \mu = J_L \cdot kT \cdot \ln\left(\frac{J_L}{J_D}\right) \tag{1}$$

where k is the Boltzmann constant (1.381×10^{-23} J K^{-1}), T in K is the temperature of the organism (assumed to be at room temperature, 295 K), J_L is the excitation rate in light (s^{-1} m^{-2}), and J_D is the thermal excitation rate (s^{-1} m^{-2}) (Ross & Calvin,

1967; Marosvölgyi & van Gorkom, 2010). In equation 1, μ, in Joules, is the potential energy of the excited pigments in the system under external illumination. Thus, P_{in} is the number of excitation events (photon absorption) generating an excited pigment multiplied by the potential chemical energy of such a pigment, μ.

The excitation rate due to the incident stellar flux, J_L, is found by dividing the incident flux into n equally sized frequency bins then multiplying by the pigment absorptance for the given frequency. The bin size should be small enough such that spectral features are not obscured. However, large discontinuities between adjacent bins can hinder convergence, which can occur if too many bins are used. Dividing the spectra in this work, which includes frequencies between ∼1200 and ∼120 THz (280 to 2500 nm), into 1200 bins preserves spectral features and does not hinder convergence. Each of these n bins represents the integrated photon flux across the frequency bin. Thus, the photon absorption is given by

$$J_L = \sum_{i=1}^{n} I_{sol,i}(1 - e^{-\tau_i}) \tag{2}$$

where τ_i is the optical depth of the pigment over the frequencies in bin i, and $I_{sol,i}$ (photons m^{-2} s^{-1}) is the integrated incident photon flux per unit area for the given frequency bin. Here, $e^{-\tau_i}$ is the transmittance, so equation 2 is the familiar description of the attenuation of external photons travelling through a medium (the cell). In this model, the photon flux with respect to frequency distribution is considered appropriate, since photosynthesis is a quantum process and frequency rather than wavelength is relevant due to the Kuhn-Reiche-Thomas sum rule for dipole transitions between electronic states (e.g. Björn, 1976).

Similar to J_L, the thermal excitation rate, J_D, is calculated across the same n frequency bins and given by

$$J_D = \sum_{i=1}^{n} \tau_i \cdot I_{bb,i} \tag{3}$$

where $I_{bb,i}$ (photons m^{-2} s^{-1}) is the integrated blackbody photon flux from the pigments at 295 K (room temperature, following Marosvölgyi & van Gorkom (2010)) per unit area for the frequency range of bin i.

The definition of J_D in equation 3 arises from two assumptions. First, it is assumed that the cell is in local thermodynamic equilibrium. Second, it is assumed that there are a sufficient number of pigments in the cell that the number of excited pigments does not appreciably deplete the number of unexcited pigments (Ross & Calvin, 1967). Under these assumptions, all photons emitted by the cell due to thermal excitation will be reabsorbed within the cell so the rate of thermal pigment excitation is equal to the rate of thermal emission. The total rate of thermal emission from the pigments in a cell is given by the number of pigments times their frequency-dependent emissivity times the frequency-dependent blackbody flux. If we assume the cell has some pigment density, n_a (pigments m^{-3}), some path length s (m), and an absorption cross section

σ_i (m^2 pigment^{-1}), then the thermal emissivity is given by $n_a \cdot s \cdot \sigma_i$ multiplied by the blackbody flux of the pigments, $I_{bb,i}$. Optical depth is defined by $\tau_i = n_a \cdot s \cdot \sigma_i$ (e.g. Catling & Kasting, 2017, §2.4.2.2), which gives equation 3.

In equations 2 and 3, we use the optical depth, τ_i, to calculate pigment excitation rates. This differs from the derivation of Marosvölgyi & van Gorkom (2010), which defined a dimensionless absorption cross-section, σ_i^*, in place of τ_i (the $*$ superscript is added here to denote the dimensionless parameter from Marosvölgyi & van Gorkom (2010)). To derive the model as described in the supplemental material of Marosvölgyi & van Gorkom (2010), σ_i^* is defined by the number of dipoles per frequency bin, g_i. That is, with units dropped, $\sigma_i^* = g_i \cdot h\nu_i \cdot B/c = d_i^* \cdot h\nu_i$ for Planck constant h, frequency ν_i, Einstein coefficient B, and speed of light c. Optical depth, which depends on σ_i, can be similarly defined by $\tau_i = g_i \cdot h\nu_i \cdot B/c \cdot n_a s = d_i \cdot h\nu_i$. The model solves for the optimal number of dipoles via d_i^*, or equivalently d_i, that maximizes photosynthetic energy production in a cell, as discussed below. Thus, using τ_i instead of σ_i^* is purely semantic and the model derivation is unchanged from the method presented in Marosvölgyi & van Gorkom (2010).

From the power input to the cell, P_{in}, which depends on τ_i through J_L and J_D, the power output from the photosynthetic apparatus is defined as P_{out}. P_{out} represents the total chemical energy stored by the cell, which accounts for energy losses from P_{in} to heat and reemission of captured photons, so $P_{out} < P_{in}$. Following Marosvölgyi & van Gorkom (2010), a simple hyperbolic relationship between P_{in} and P_{out} is assumed and that P_{out} saturates at some power output, P_{sat}. With these assumptions, P_{out} is given by

$$P_{out} = \frac{1}{1/P_{in} + 1/P_{sat}}. \tag{4}$$

The saturation term in equation 4, P_{sat}, is necessary to account for the diminishing energy output per pigment as a cell becomes increasingly absorbent. For example, a black cell that absorbs all incoming photons will not harvest more photon energy by creating additional pigments and has thus reached the saturation point for power output.

The proteins required to build these photosynthetic pigments and the subsequent chemical storage of the captured energy must have some cost to the cell. Following Marosvölgyi & van Gorkom (2010), we define $C_{P_{in}}$ as the dimensionless fractional energetic cost to the cell to create the light-harvesting machinery. Similarly, $C_{P_{out}}$ is defined as the fractional cost to the cell to create the mechanism necessary to store the captured photon energy. The remaining fractional energy, that is the relative energy not spent on light harvesting and subsequent storage, is spent driving cellular growth, C_G, or $C_G = 1 - C_{P_{in}} - C_{P_{out}}$.

With the cellular costs $C_{P_{in}}, C_{P_{out}}$, and C_G defined, the growth power available to the cell, P_G, is simply defined as

$$P_G = P_{out} \cdot C_G = P_{out} \cdot (1 - C_{P_{in}} - C_{P_{out}}). \tag{5}$$

We want to find the number of dipoles in each frequency bin, that is the d_i, that maximize P_G. This maximum will occur when the gradient of P_G with respect to d_i is 0, i.e. $\partial P_G/\partial d_i = 0$. The derivation of $\partial P_G/\partial d_i$ is carried out in detail in the supplemental material of Marosvölgyi & van Gorkom (2010) and produces n equations (recall that n is the number of frequency bins) with the form

$$I_{sol,i} \cdot h\nu_i \cdot e^{-\tau_i} = \frac{kT \cdot e^{\mu/(kT)} \cdot h\nu_i}{\mu + kT} \cdot I_{bb,i} + \frac{P_{in}}{(\mu + kT) \cdot \sum_{j=1}^{n} \tau_j/(h\nu_j)} \cdot \frac{C_{P_{in}}}{C_{P_{in}} + C_G}. \quad (6)$$

In equation 6, h is the Planck constant (6.626×10^{-34} J s) and $C_{P_{in}}/(C_{P_{in}} + C_G)$, which we define as $C = C_{P_{in}}/(C_{P_{in}} + C_G)$, is the *relative cost parameter* that represents the ratio of the cost of the light harvesting machinery to the sum of the light harvesting and fractional growth energies (Marosvölgyi & van Gorkom, 2010). C is a free parameter in the model and $0 \leq C \leq 1$. When $C = 0$, there is no cost to the cell to create photosynthetic pigments leaving all energy to drive growth. When $C = 1$, all absorbed energy is spent creating the photosynthetic pigments and no energy is available for growth.

The left-hand side of equation 6 is the transmitted photon energy and is balanced by two terms on the right-hand side (RHS). The first term on the RHS of equation 6 is the scaled blackbody flux of the pigment. This term sets the frequency below which pigments would emit more energy than they absorb and results in an abrupt transition to a transmittance of 1 below the cutoff frequency. This frequency cutoff is analogous to the bandgap in photovoltaic semiconductors (Marosvölgyi & van Gorkom, 2010) and depends on the incident stellar photon flux.

The second term on the RHS of equation 6 imposes an input energy threshold on the frequencies at which a pigment can absorb (Marosvölgyi & van Gorkom, 2010). This term is spectrally constant but depends on C. As $C \to 0$, this term goes to 0 causing the spectral bins below the bandgap frequency to absorb all available photons. As C increases from 0, only the spectral bins where energy input to the cell relative to thermal emission is largest continue to absorb. These high-energy input bins represent the most efficient frequencies for absorption as we assume pigment creation costs have no spectral dependence. Thus, C can analogously be considered a measure of pigment efficiency. As C increases, pigment absorption in inefficient parts of the spectrum is precluded and only remains at frequencies where stellar photon energy is abundant. This is readily seen in Figure 1, which shows the predicted absorptance spectrum of an optimized cell from equation 6 for the modern Earth around the Sun with various C values between 0 and 1.

Equation 6 is a fixed-point equation that can be solved for τ_i with iterative mapping. For a given relative cost parameter, C, an initial guess for each τ_i is provided, then equation 6 is iterated until convergence is reached. For values of C near 0 or 1, the initial guess for each τ_i must be close to the solution for the model to converge. Therefore, we initially run the model with an intermediate value for C (such as $C = 0.5$) and initialize

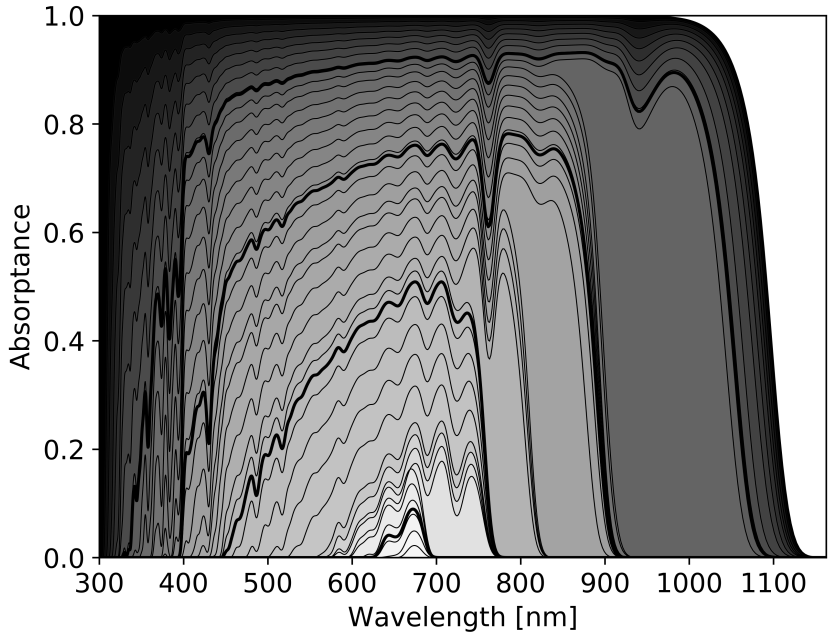

Figure 1: The optimal pigment absorptance spectrum for different cost parameters around the Sun, a G2V star. The horizontal axis shows wavelength in nm, the vertical axis shows pigment absorptance. Each black curve shows the predicted pigment absorptance for the given cost parameter, C from equation 6. The value of C is indicated by the shading where darker shading indicates lower cost. Black shading corresponds to no cost, i.e. $C = 0$; shading approaches white as the cost increases, i.e. $C \to 1$. The bold black contours show, from top to bottom, a C value of 0.25, 0.5, 0.75, and 0.962, respectively. The predicted absorptance spectrum was smoothed by convolution with a 10 nm wide Gaussian function. As C increases, the optimal absorptance spectra focuses to spectral regions where high-energy photons are most abundant. This figure recreates the results of Marosvölgyi & van Gorkom (2010), see their Figure 2.

each τ_i to 1 then iterate equation 6 to convergence. With the converged solution for each τ_i at the intermediate C value, we iterate over C to $C = 1$ or $C = 0$ using the previously converged solution for each τ_i as inputs to equation 6 for the next value of C. In this way, equation 6 converges for all C values between 0 and 1, including the end points.

The effect of changing C on the optimal pigment absorbance spectrum from equation 6 is shown in Figure 1. As C increases, equation 6 predicts pigment absorption should focus on spectral regions where the balance between photon absorption and thermal emission maximizes energy input to the cell. Thus, pigment absorbance spectra should jump across atmospheric absorption bands. This is readily seen in Figure 1, where jumps in predicted pigment absorptance correspond to atmospheric absorption features, such as those of O_2 at 688 and 761 nm and from H_2O at 720, 820, and 940 nm (Hill & Jones, 2000; Kiang et al., 2007b).

As wavelength increases, blackbody emission of the organism becomes increasingly important. Even in the scenario $C = 0$, no pigment absorption is predicted beyond ∼1100 nm for the modern Earth around the Sun. Beyond this wavelength, there are insufficient photons to make up for the emissions from the pigments. Thus, in this model, pigments cannot absorb beyond ∼1100 nm without a loss of energy. This limit agrees with extant Earth organisms and theoretical calculations of the long-wavelength limit of light-driven energy production (Marosvölgyi & van Gorkom, 2010). For different stellar types this limit will change based on the incident flux of infrared photons, as shown in Appendix A.1. We note that other limitations on the long-wavelength limit for oxygenic photosynthesis may exist (e.g. Kiang et al., 2007b; Lehmer et al., 2018), but no such limits are imposed in the model presented here.

The relative cost parameter, C, can be freely tuned in the model. However, a relative cost of $C = 0.962$, indicating only the most efficient frequency bins should absorb photons, reproduces the red absorption feature of spinach chloroplasts. Furthermore, the same C applied to the ambient spectra in a muddy water column reproduces the absorption position and shape of the *Rhodobacter sphaeroides* chromatophores (Marosvölgyi & van Gorkom, 2010). Following Marosvölgyi & van Gorkom (2010), we assume $C = 0.962$ is applicable to photosynthetic organisms generally. However, lab measurements of additional photosynthetic organisms are necessary to know if $C = 0.962$ is universally applicable for Earth-based life or if a range of C values may be appropriate.

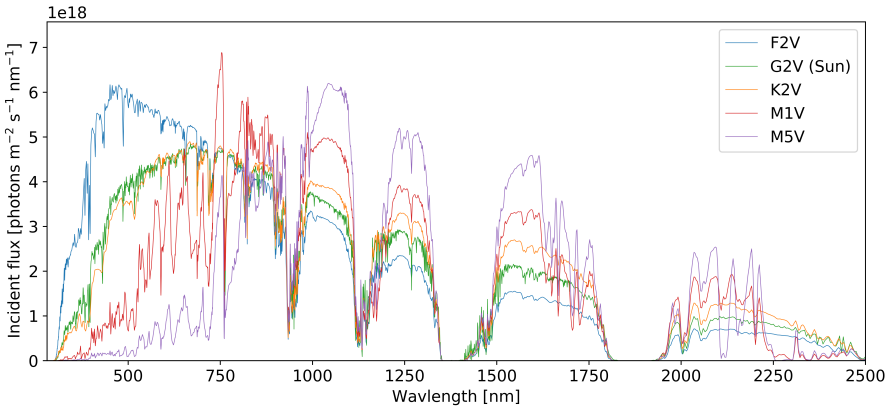

Figure 2: The surface spectral photon flux for planets with modern Earth-like CO_2, N_2, O_2, and surface-to-atmosphere reactive gas fluxes that are equilibrated with the spectral radiation of different parent stellar types (see text for details). The horizontal axis shows photon wavelength in nm, the vertical axis shows the incident photon flux per unit area, per second, per nm. Each colored contour shows the surface photon flux for a different stellar type, as labelled. For each stellar type, the total stellar flux corresponds to a mean planetary surface temperature of 288 K. The photon flux for the Sun is from ASTM (2020). All other spectra are from Kiang et al. (2007b).

As inputs to the model, we use the standard solar irradiance spectrum for the modern Earth at sea level from ASTM (2020). We also consider simulated surface

spectra from Kiang et al. (2007b) around F2V, K2V, M1V, and M5V type stars. For simulated spectra around other stars, the atmosphere was assumed to be 1 bar with O_2, CO_2, and N_2 mixing ratios equivalent to modern Earth's. For fixed O_2, the atmospheric compositions were photochemically evolved to equilibrium based on the incident stellar irradiance spectrum (see Kiang et al. (2007b) for details). The spectra considered in this work are shown in Figure 2.

3 Results

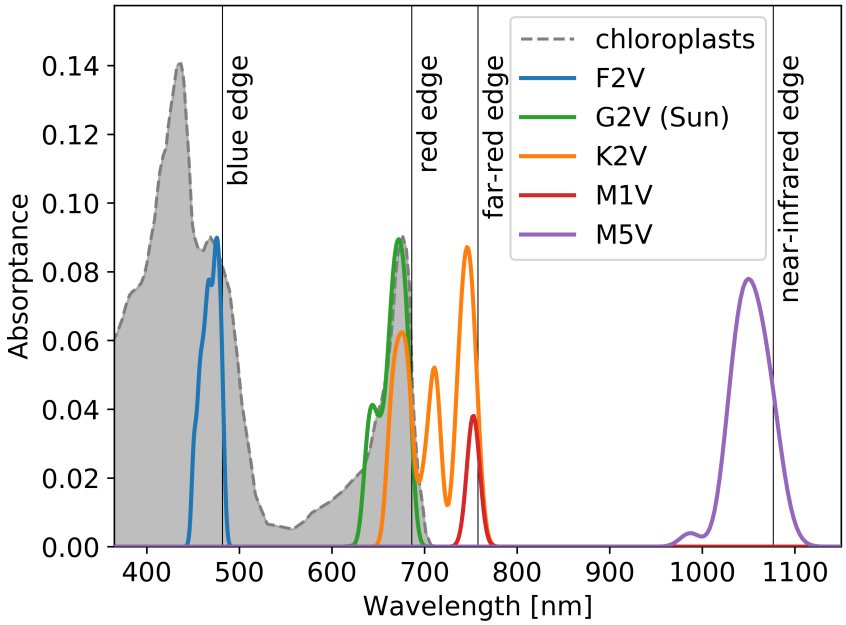

Figure 3: The optimal pigment absorbance spectrum for each stellar type from our pigment optimization model (see Section 2). The horizontal axis shows wavelength in nm. The vertical axis shows the predicted absorptance of pigments from the model. Each colored contour represents a different stellar type, as labelled. The shaded gray region and dashed gray line show the absorptance of spinach chloroplasts from Marosvölgyi & van Gorkom (2010), arbitrarily normalized to match the vertical extent of the optimal pigment profile for Earth. The absorbance spectra were smoothed by convolution with a 10 nm wide Gaussian function, following Marosvölgyi & van Gorkom (2010). The model predicts the wavelength of peak absorption and the corresponding absorption shape around that peak. The total absorptance of an organism is not reflected by the vertical axis. An organism could produce additional pigments to boost total absorptance, but the optimized absorption peak and shape would remain the same. The position of and shape of Chl *a* absorption at ~680 nm (dashed gray contour) is predicted in both location and shape by the model (green contour). The reflectance edges that future telescopes might search for are shown by the vertical black lines and corresponding labels.

Table 1: The model predicted absorptance peaks for each stellar type shown in Figure 3.

Stellar Type	Absorptance Peaks [nm]
F2V	468, 476
G2V (Sun)	644, 672
K2V	675, 711, 746
M1V	753
M5V	987, 1050

From the spectra in Figure 2, Figure 3 shows the predicted absorbance spectrum for optimal pigments around each stellar type. The gray shaded region shows the absorbance spectrum of spinach chloroplasts from Marosvölgyi & van Gorkom (2010), which matches the predicted absorbance spectrum in the Q_y band of *in vivo* Chl *a* on Earth (green contour in Figure 3). The green contour in Figure 3 reproduces the results of Marosvölgyi & van Gorkom (2010). It is important to note in Figure 3 that the absolute absorptance value predicted by the model is not necessarily representative of the total absorptance of an organism. The model predicts an optimal absorption wavelength and profile over wavelength, but an organism could produce multiple copies of the optimal pigment, which would alter the absolute absorptance of the organism.

The optimized absorptance peaks shown in Figure 3 are listed in Table 1 and agree with the qualitative predictions from Kiang et al. (2007b). In addition to predicting the absorptance peaks, we also predict the shape of the absorbance spectra around each peak and, depending on stellar type, multiple absorptance peaks. The shapes of the absorptance peaks depend on the incident stellar flux, atmospheric absorption, and the relative cost parameter. The broad absorptance peak predicted for an M5V star arises due to abundant available photons near 1050 nm with limited atmospheric attenuation around that peak. Stronger atmospheric absorption features near the absorptance peaks for the other stellar types restrict the width of the predicted absorptance peaks.

The optimal absorbance spectra depend on the relative cost parameter, C, and the total available stellar photon flux for absorption, as demonstrated in Figure 4. As gray contours, Figure 4 shows the model predicted optimal absorbance spectra for 6 different values of $C \in \{0.90, 0.92, 0.94, 0.962, 0.98, 0.99\}$ at the inner and outer edges of the habitable zone (HZ). The $C = 0.962$ contour is highlighted in black. As a first-order approximation, the photon fluxes available at the inner and outer edges of the HZ for each stellar type are calculated by linearly scaling the photon fluxes from Figure 2 by the HZ flux limits in Table 2. The HZ flux limits considered in Figure 4 do not take into account environmental and atmospheric changes that may occur by moving an Earth-like planet between the inner and outer edges of the HZ. Thus, the results shown in Figure 4 are only illustrative of how changes in total stellar flux alone could influence optimal pigment absorption profiles.

In the outer HZ, the decreased total stellar flux can push the optimal absorbance

Table 2: The normalized incident fluxes, S, at the inner and outer edges of the habitable zone (HZ) for each stellar type. The HZ flux limits are normalized to the incident flux of the modern Earth ($S_\oplus = 1360$ W m^{-2}) and taken from Kopparapu et al. (2013).

Stellar Type	Temperature [K]	Inner Edge $[S/S_\oplus]$	Outer Edge $[S/S_\oplus]$
F2V	7120	1.11	0.41
G2V (Sun)	5780	1.01	0.34
K2V	4620	0.93	0.28
M1V	3330	0.86	0.23
M5V	2670	0.84	0.21

peak wavelength toward shorter wavelengths when C is low. This is readily seen for the $C = 0.90$ curve of the M1V star in Figure 4. In the inner HZ of this star at $C = 0.90$, pigments are optimal when absorbing beyond 1000 nm. However, in the outer HZ, absorption at 1000 nm is precluded as there are insufficient long-wavelength stellar photons to overcome thermal emission of the pigments. As C increases, optimal pigment absorption focuses around the most energetically favorable wavelengths and the change in total stellar flux between the inner and outer limits of the HZ has limited influence on optimal pigment absorption wavelength, as seen in Figure 4.

The predicted optimal absorbance spectra for each stellar type shows the influence of atmospheric absorption on pigment optimization. Comparing the input spectra in Figure 2 to the predicted absorbance wavelengths in Figures 3, we see that atmospheric absorption features, particularly from H_2O at 720, 820, 940, and 1130 nm (Hill & Jones, 2000; Kiang et al., 2007b), exert a strong pressure on pigments to absorb in atmospheric windows. In addition, short-wavelength, high-energy photons in the visible (and just beyond) provide maximum growth energy for organisms around F, G, K, and even early M stars. Only around the coolest M5V star are organisms optimized when absorbing well into the NIR. These predictions may better inform the search for red edge analogs around other stars, as discussed below.

See Appendix A.2 for plots comparing the different stellar spectrum and corresponding predictions for optimal pigment absorptance.

4 Discussion

If we are to detect a sharp change in reflectance spectra from alien, photosynthetic organisms, i.e., a red edge analog, knowing the exact wavelengths to observe is critical as the spectral signal may be small (Sagan et al., 1993; Seager et al., 2005; Kiang et al., 2007a; O'Malley-James & Kaltenegger, 2018; Wang & He, 2021). In this work, the goal of predicting pigment absorbance spectra is to inform the wavelength ranges future observations should preferentially consider for detection of a red edge analog.

On the modern Earth, the red edge in the NIR corresponds to the steep drop in

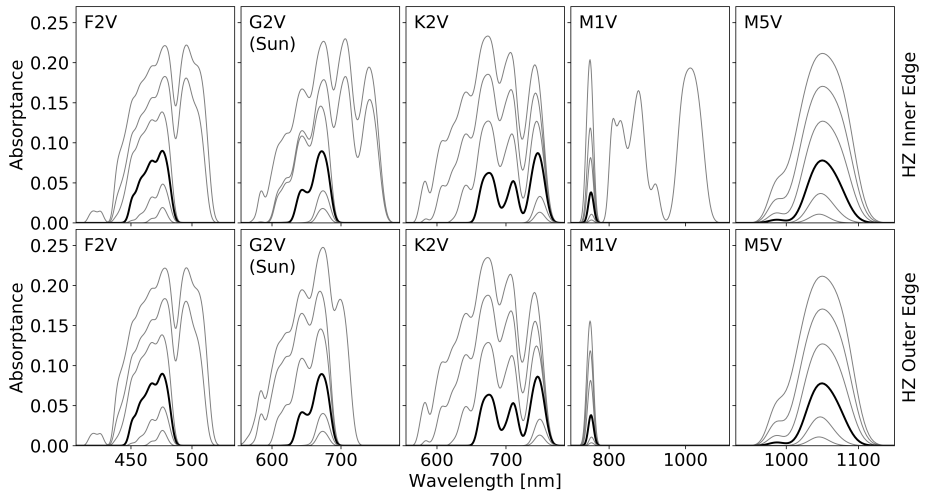

Figure 4: The optimal pigment absorptance predicted by the model for each stellar type for irradiance intensities approximately spanning the inner and outer edges of the habitable zone (HZ) for various relative cost parameters, C. From top to bottom, the contours in each figure correspond to a C value of: 0.90, 0.92, 0.94, 0.962, 0.98, 0.99. The 0.962 contour is shown in bold black while all other contours are in gray. The top row of plots shows the optimal pigment absorptance profile at the inner edge of the HZ, the bottom row at the outer edge. The flux values used for the inner and outer edge of the HZ are given in Table 2. For $C \geq 0.94$ the predicted absorptance profile is the same throughout the HZ for all stellar types. At lower C values, the optimal absorptance profile can change between the inner and outer edges of the HZ due to changes in total incident flux, as shown by the $C = 0.90$ contour for the M1V star.

absorption beyond the optimal peak of Chl *a* (gray shaded region in Figure 3). If photosynthetic organisms around other stars exhibit similar edge-like spectral reflectance features, we might expect red edge analogs to occur on the long-wavelength side of the optimal pigment absorption, similar to the prediction of Tinetti et al. (2006).

The wavelength of optimal pigment absorption will depend on both the atmospheric composition and the photon flux of the host star. Both stars and planetary atmospheres evolve with time (e.g. Bahcall et al., 2001; Lyons et al., 2014), so the optimal wavelength for pigment absorption may also evolve with time. For the Sun, changes in luminosity with time have not led to significant spectral change across the photosynthetically active radiation wavelengths (Claire et al., 2012). In addition, from Figure 4, we see that changes in total stellar flux do not alter the optimal pigment absorption wavelengths except at low values of C; lower values of C could also result as adaptations to low light, as seen in the far-red and low-light adapted cyanobacterium *Acaryochloris marina* (Mielke et al., 2011). Thus, for the Earth through time, changes in atmospheric composition could regulate optimal pigment absorption wavelengths.

Atmospheric compositions on habitable exoplanets could be very different from modern Earth's (e.g. Segura et al., 2003, 2005; Schwieterman et al., 2018), which would

filter radiation and alter the surface spectral irradiance (Kiang et al., 2007b) to which optimal wavelengths for pigments absorption would be adapted. A relationship between available photon fluxes and pigment absorption profiles is well established on the modern Earth (see Introduction) and is even found in photoautotrophs where accessory pigments rather than the trap pigment dominate the spectral light absorbance. For example, the anoxygenic photosynthetic bacterium *Blastochloris viridis* has a bacteriochlorophyll *b* trap wavelength at 960 nm where the underwater photon flux in this organism's environment is low, while core antenna pigments provide higher absorbance at ∼890 and 1015 nm (the latter actually being up the energy hill from the trap) where photons are more abundant (Kiang et al., 2007b). The model used here predicts an optimal pigment absorption profile based on the available photon flux and does not differentiate between trap and accessory pigments.

As mentioned earlier, land plants have abundant accessory pigments throughout the visible spectrum. Indeed, green plants absorb almost all visible photons, including ∼95% of green photons (e.g. Björn et al., 2009), with the help of these accessory pigments. It is not surprising that green land plants contain these accessory pigments. If Chl *a* bearing organisms were limited to the narrow range of photons around the absorption peak at ∼680 nm, say photons between 670 and 690 nm, $\sim 9 \times 10^{19}$ photons m^{-2} s^{-1} would be available from the spectra in Figure 2 for the Earth around the Sun. To first order, this is only $\sim \frac{1}{4}$ of the current photon use by the terrestrial biosphere (3.26×10^{20} photons m^{-2} s^{-1}) (Field et al., 1998; Lehmer et al., 2018). Without accessory pigments, terrestrial, Chl *a*-bearing organisms would not be fully exploiting available light and potential growth. Instead, land plants appear to have adapted by adding (or losing) accessory pigments until photon absorption is no longer growth limiting and nutrient availability, often bioavailable phosphorous or nitrogen (Tyrrell, 1999; Reinhard et al., 2016), or water availability on land (Porporato et al., 2002, 2003), limits growth.

In addition to absorption of short-wavelength photons from accessory pigments, large pigments, such as Chl *a*, should have auxiliary, short-wavelength absorption features (e.g. Papageorgiou, 2004). Pigments like Chl *a* must be sufficiently large that their π-electrons can be excited by long-wavelength photons at the edge of the visible spectrum (Mauzerall et al., 1976). This large structure results in additional absorption features from higher energy electron orbitals (e.g. Björn et al., 2009). So the absorption of blue photons by Chl *a*, which provides additional photon harvesting for a Chl *a*-bearing organism similar to an accessory pigment, may be a side-effect of the structure of Chl *a* being tuned to optimally absorb in the red rather than a feature that was selected for (Marosvölgyi & van Gorkom, 2010), but see Arp et al. (2020) for an alternative explanation.

If alien photoautotrophs have abundant accessory pigments and auxiliary, short-wavelength absorption features in their pigments, as occur on Earth, Earth-like planets around the stars considered here would have sufficient spectral energy to sustain the Earth's extant biosphere. If we assume photons longer than 300 nm may be used by photosynthetic organisms (McCree, 1971), more than double the current photon

use of the terrestrial biosphere is available for each stellar type shown in Figure 2. This assumes absorption only occurs between 300 nm and the optimal wavelength shown in Figure 3. Even if we account for the reduced quantum yield of the M5V pigment, which may be ∼50% as productive due to the lower quantum yield of low-energy, long-wavelength photons (Wolstencroft & Raven, 2002; Kiang et al., 2007b; Lehmer et al., 2018), no spectral energy limitation on growth is encountered, although the total stellar flux may be a constraint around the coolest of stars (Lehmer et al., 2018). Thus, it may be unlikely for an organism to produce pigments absorbing beyond the optimal pigment absorption wavelength. Such pigments may need to be large to absorb the longer wavelength photons (Mauzerall et al., 1976) and thus could be costly for the cell to build. In addition, these pigments would absorb lower-energy photons and potentially have a lower quantum yield compared to accessory pigments at short wavelengths, where photons are still abundant.

The full reflectance spectra of an organism is derived not only from its pigments. As noted by Kiang et al. (2007b), cellular structure, and in the case of land plants, canopy structure and leaf morphology could play important roles in determining the reflectance spectra and thus the red edge. These aspects are not considered in our model so the discussion of the alien red edge analog location should be considered approximate. However, given the lack of understanding on how these other properties may alter the red edge around different stars (Kiang et al., 2007b), we propose the optimal absorption peak is a reasonable initial location to search for a vegetative red edge analog, as is the case on the modern Earth.

5 Conclusion

Future exoplanet observations may search for a vegetative red edge equivalent, a spectral signature due to a sharp slope in the reflectance of photosynthetic organisms (e.g. Sagan et al., 1993; Seager et al., 2005; Kiang et al., 2007b; O'Malley-James & Kaltenegger, 2018; Wang & He, 2021). The wavelength where a red edge analog occurs on other planets will likely depend on the stellar type, as seen in Figure 3. Here, we only consider atmospheric compositions with CO_2, N_2, and O_2 similar to the modern Earth that are photochemically equilibrated with the incident stellar photon flux (see Methods), but different atmospheric compositions could also change the wavelength of red edge analogs by altering the availability of surface photons (e.g. Kiang et al., 2007b; Arney et al., 2016). Direct imaging mission concepts, such as NASA's HabEx and LUVOIR, could constrain the atmospheric composition and thus the surface photon flux of habitable worlds and search for a vegetative red edge analog based on that measurement, as modeled here.

The exact nature of oxygenic photosynthesis, why certain absorption features exist and what drives accessory pigment production remains under investigation (e.g. see reviews Björn et al., 2009; Björn & Ghiradella, 2015). However, the model described in this work and similar models can explain the absorption features, at least in part,

of numerous extant Earth organisms (Björn, 1976; Stomp et al., 2007; Kiang et al., 2007a; Milo, 2009; Marosvölgyi & van Gorkom, 2010). An edge-like photosynthetic pigment signature on an extrasolar planet will depend on the context of the parent star, atmosphere, and evolutionary stage of the planet. If evolution of photosynthesis tends always toward maximizing power gain, then the most likely candidate for a photosynthetic red edge analog on habitable exoplanets occurs at the optimal absorption peak, as depicted in Figure 3 for a selection of stellar types.

Acknowledgements

We would like to thank NASA's Virtual Planetary Laboratory (grant 80NSSC18K0829) at the University of Washington and the NASA Pathways Program at the NASA Ames Research Center for funding this work.

A Supplemental figures

A.1 Cost Parameter Variations

Figure 1 shows how changes in the relative cost paramter, C, change the optimal abosrbance profile predicted from equation 6 for photosythetic organisms on the modern Earth around the Sun. In this section, we reproduce Figure 1 for the spectra from each stellar type shown in Figure 2. Around each stellar type, the optimal aborbance profile jumps atmospheric absorption features, similar to Figure 1. The long-wavelength limit for absorption, where thermal emission precludes pigment absorption, changes based on stellar type.

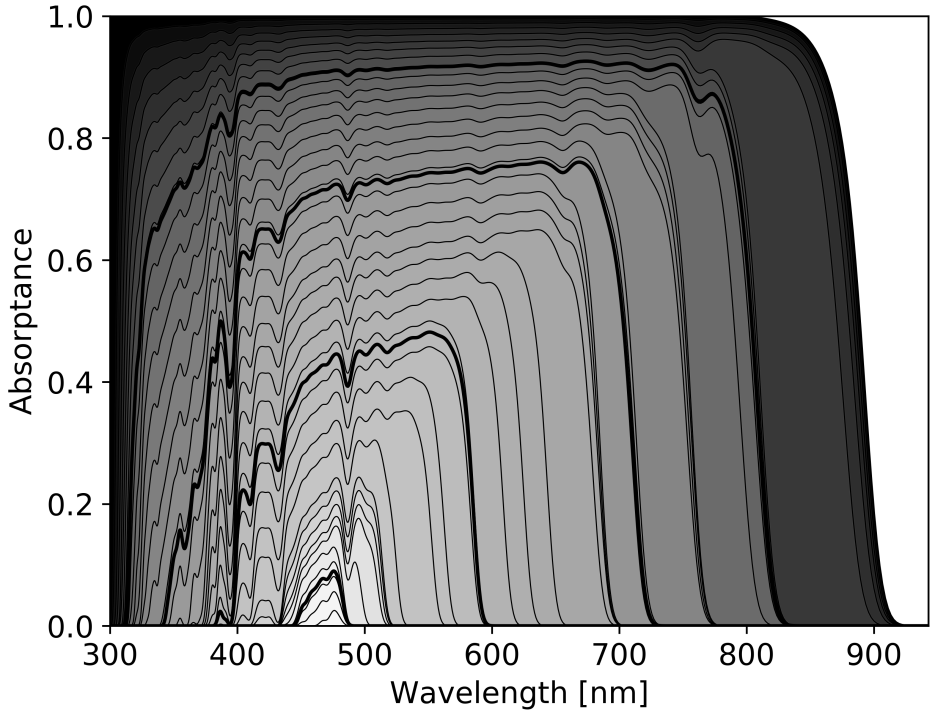

Figure 5: The optimal pigment absorbance spectrum for different cost parameters around an F2V star. See Figure 1 (an equivalent plot for the Sun) for a full description.

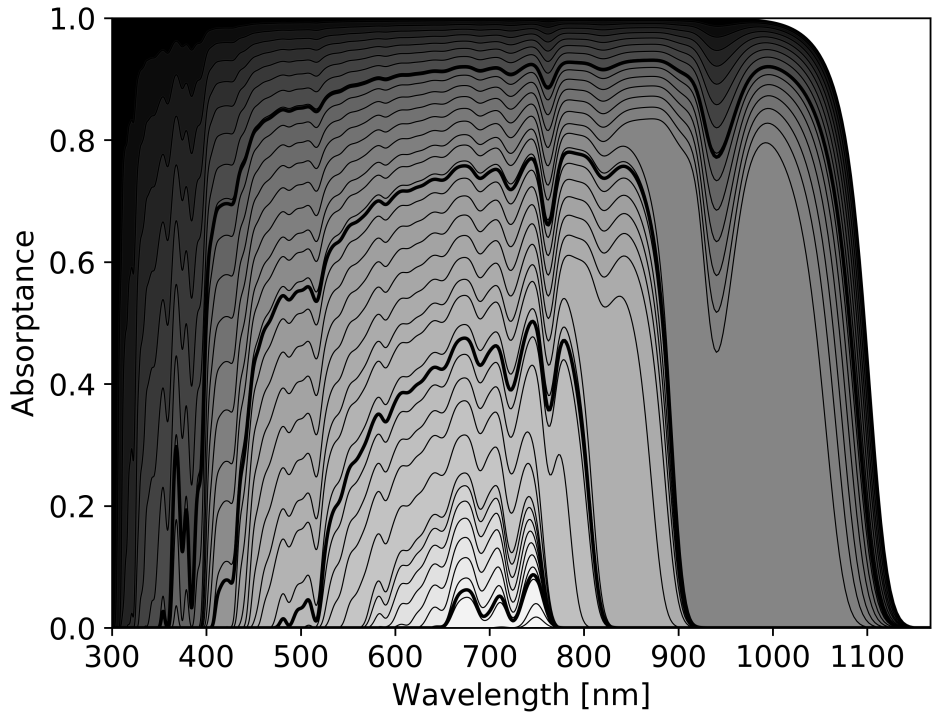

Figure 6: The optimal pigment absorbance spectrum for different cost parameters around an K2V star. See Figure 1 (an equivalent plot for the Sun) for a full description.

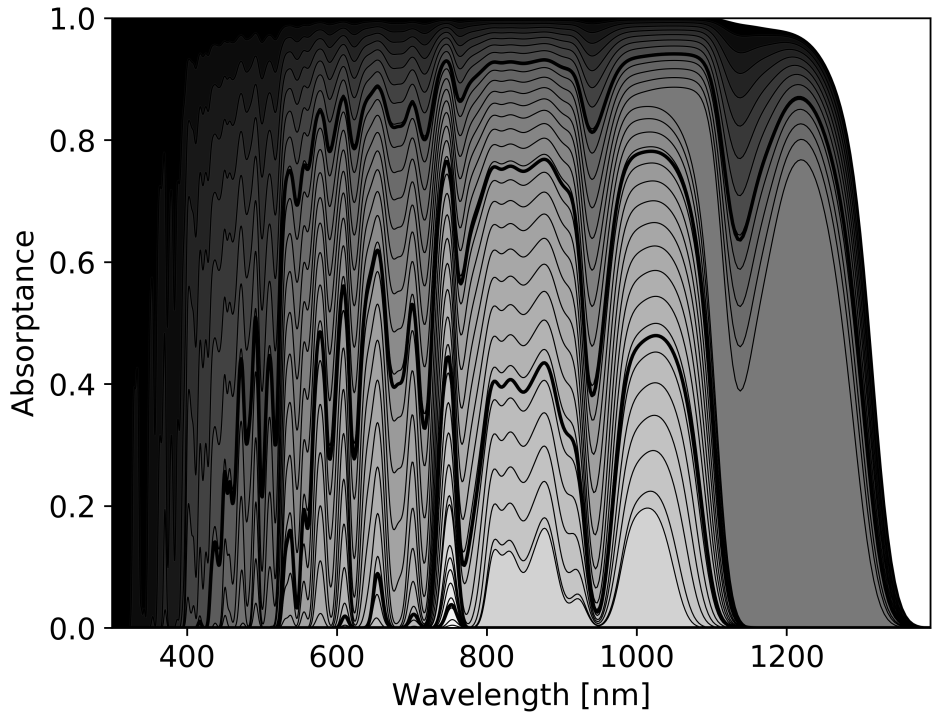

Figure 7: The optimal pigment absorbance spectrum for different cost parameters around an M1V star. See Figure 1 (an equivalent plot for the Sun) for a full description.

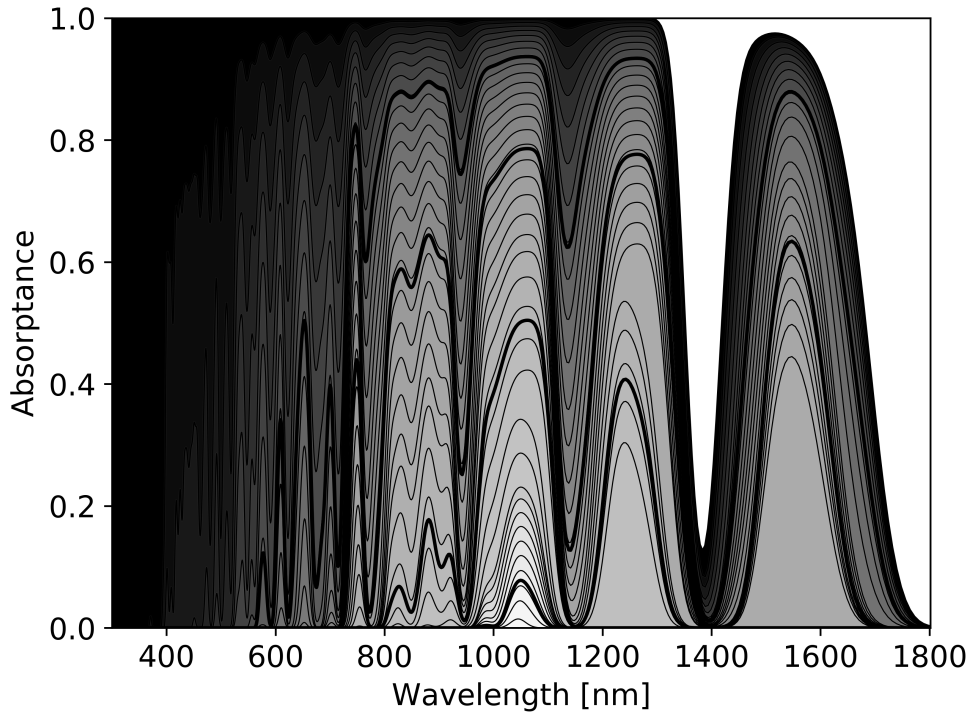

Figure 8: The optimal pigment absorbance spectrum for different cost parameters around an M5V star. See Figure 1 (an equivalent plot for the Sun) for a full description.

A.2 Individual Spectra

The incident photon fluxes for each stellar type considered in this work (Figure 2) are shown in Figures 9, 10, 11, 12, and 13 with the corresponding prediction for pigment absorptance from Figure 3. The contours in these figures are the same contours as shown in Figure 2 and Figure 3, but shown individually for clarity. In each figure, the vertical scaling of the predicted pigment absorptance profile is arbitrary. Only the wavelength of the absorptance peak and the absorbance spectra around that peak are important.

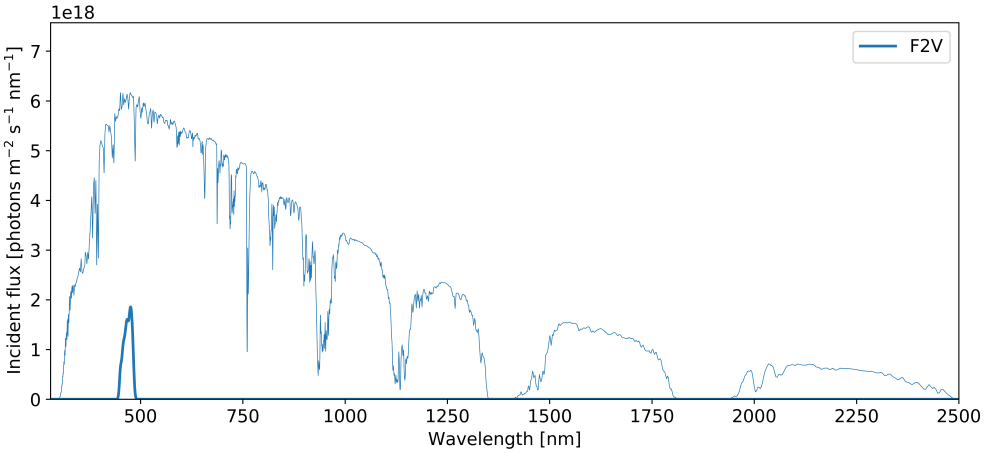

Figure 9: The predicted optimal pigment absorbance spectrum for an F2V star. The curves shown here are from Figures 2 and 3.

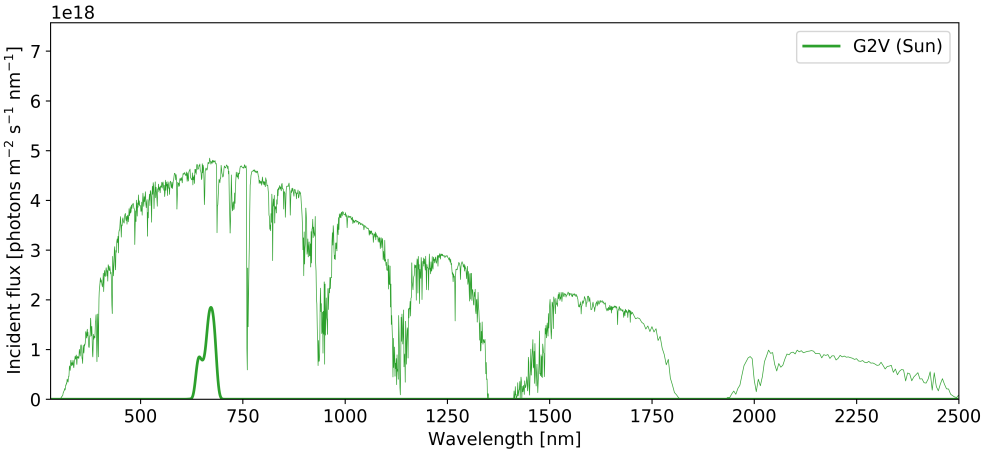

Figure 10: The predicted optimal pigment absorbance spectrum for an G2V star. The curves shown here are from Figures 2 and 3.

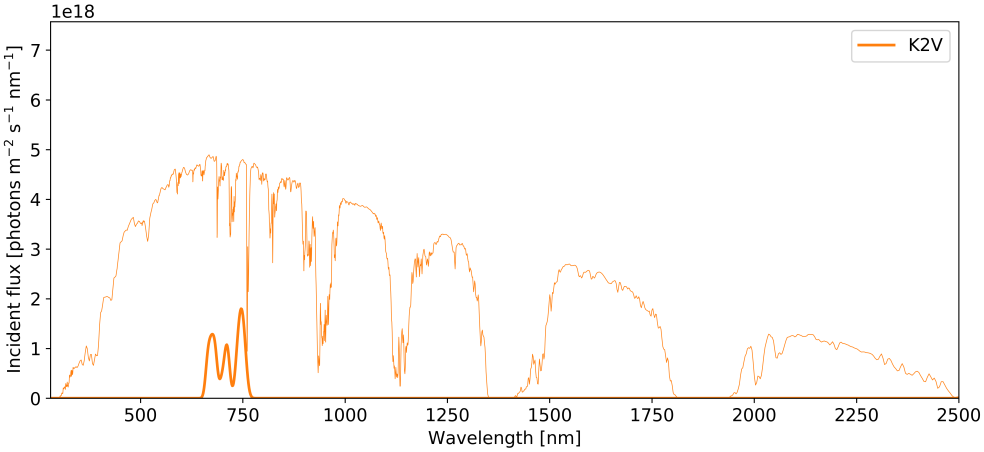

Figure 11: The predicted optimal pigment absorbance spectrum for an K2V star. The curves shown here are from Figures 2 and 3.

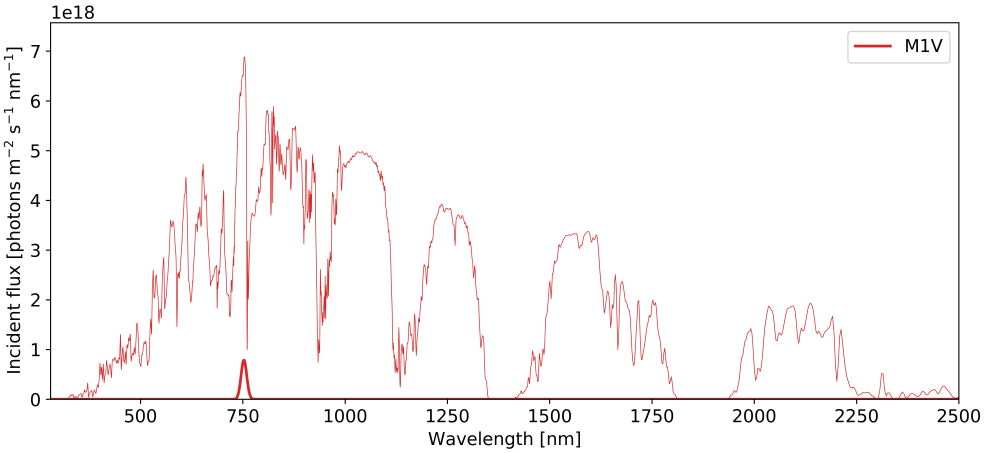

Figure 12: The predicted optimal pigment absorbance spectrum for an M1V star. The curves shown here are from Figures 2 and 3.

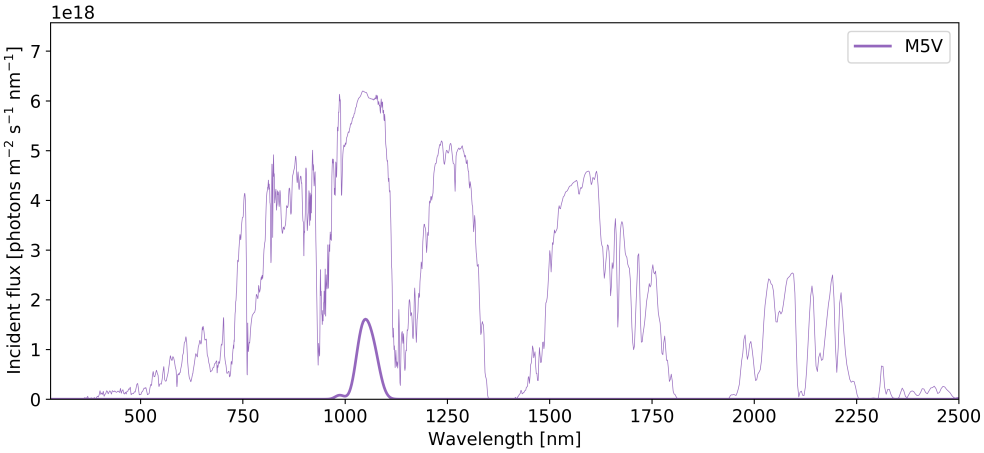

Figure 13: The predicted optimal pigment absorbance spectrum for an M5V star. The curves shown here are from Figures 2 and 3.

References

Arney, G., Domagal-Goldman, S. D., Meadows, V. S., et al. 2016, The Pale Orange Dot: The Spectrum and Habitability of Hazy Archean Earth, Astrobiology, 16, 873, doi: 10.1089/ast.2015.1422

Arp, T. B., Kistner-Morris, J., Aji, V., et al. 2020, Quieting a noisy antenna reproduces photosynthetic light-harvesting spectra, Science, 368, 1490, doi: 10.1126/science.aba6630

ASTM. 2020, Reference Air Mass 1.5 Spectra | Grid Modernization | NREL. https://www.nrel.gov/grid/solar-resource/spectra-am1.5.html

Bahcall, J. N., Pinsonneault, M. H., & Basu, S. 2001, Solar Models: Current Epoch and Time Dependences, Neutrinos, and Helioseismological Properties, The Astrophysical Journal, 555, 990, doi: 10.1086/321493

Björn, L. O. 1976, Why are plants green - relationships between pigment absorption and photosynthetic efficiency, Photosynthetica, 10, 121. http://lup.lub.lu.se/record/134648

Björn, L. O., & Ghiradella, H. 2015, in Photobiology, ed. L. O. Björn (New York, NY: Springer New York), 97–117, doi: 10.1007/978-1-4939-1468-5_9

Björn, L. O., Papageorgiou, G. C., Blankenship, R. E., & Govindjee. 2009, A viewpoint: Why chlorophyll a?, Photosynthesis Research, 99, 85, doi: 10.1007/s11120-008-9395-x

Blankenship, R. E. 2008, in Molecular Mechanisms of Photosynthesis (Blackwell Science Ltd), 1–10, doi: 10.1002/9780470758472.ch1

Blankenship, R. E. 2014, Molecular Mechanisms of Photosynthesis (United Kingdom: John Wiley & Sons)

Catling, D. C., & Kasting, J. F. 2017, Atmospheric Evolution on Inhabited and Lifeless Worlds (New York: Cambridge University Press)

Claire, M. W., Sheets, J., Cohen, M., et al. 2012, The Evolution of Solar Flux From 0.1 nm to 160 microns: Quantitative Estimates for Planetary Studies, The Astrophysical Journal, 757, 95, doi: 10.1088/0004-637X/757/1/95

Field, C. B., Behrenfeld, M. J., Randerson, J. T., & Falkowski, P. 1998, Primary production of the biosphere: integrating terrestrial and oceanic components, Science, 281, 237. http://science.sciencemag.org/content/281/5374/237.short

Gausman, D. H. 1974, Leaf Reflectance of Near-lnfrared, Photogrammetric Engineering, 40, 183

Hill, C., & Jones, R. L. 2000, Absorption of solar radiation by water vapor in clear and cloudy skies: Implications for anomalous absorption, Journal of Geophysical Research: Atmospheres, 105, 9421, doi: 10.1029/1999JD901153

Kiang, N. Y., Siefert, J., Govindjee, & Blankenship, R. E. 2007a, Spectral Signatures of Photosynthesis. I. Review of Earth Organisms, Astrobiology, 7, 222, doi: 10.1089/ast.2006.0105

Kiang, N. Y., Segura, A., Tinetti, G., et al. 2007b, Spectral Signatures of Photosynthesis. II. Coevolution with Other Stars And The Atmosphere on Extrasolar Worlds, Astrobiology, 7, 252, doi: 10.1089/ast.2006.0108

Kopparapu, R. K., Ramirez, R., Kasting, J. F., et al. 2013, Habitable Zones around Main-sequence Stars: New Estimates, The Astrophysical Journal, 765, 131, doi: 10.1088/0004-637X/765/2/131

Lehmer, O. R., Catling, D. C., Parenteau, M. N., & Hoehler, T. M. 2018, The Productivity of Oxygenic Photosynthesis around Cool, M Dwarf Stars, The Astrophysical Journal, 859, 171, doi: 10.3847/1538-4357/aac104

Lyons, T. W., Reinhard, C. T., & Planavsky, N. J. 2014, The rise of oxygen in Earth's early ocean and atmosphere, Nature, 506, 307, doi: 10.1038/nature13068

Marosvölgyi, M. A., & van Gorkom, H. J. 2010, Cost and color of photosynthesis, Photosynthesis Research, 103, 105, doi: 10.1007/s11120-009-9522-3

Mauzerall, D., Neuberger, A., & Kenner, G. W. 1976, Chlorophyll and photosynthesis, Philosophical Transactions of the Royal Society of London. B, Biological Sciences, 273, 287, doi: 10.1098/rstb.1976.0014

McCree, K. J. 1971, The action spectrum, absorptance and quantum yield of photosynthesis in crop plants, Agricultural Meteorology, 9, 191

Mielke, S., Kiang, N., Blankenship, R., Gunner, M., & Mauzerall, D. 2011, Efficiency of photosynthesis in a Chl d-utilizing cyanobacterium is comparable to or higher than that in Chl a-utilizing oxygenic species, Biochimica et Biophysica Acta (BBA) - Bioenergetics, 1807, 1231, doi: 10.1016/j.bbabio.2011.06.007

Milo, R. 2009, What governs the reaction center excitation wavelength of photosystems I and II?, Photosynthesis Research, 101, 59, doi: 10.1007/s11120-009-9465-8

O'Malley-James, J. T., & Kaltenegger, L. 2018, The Vegetation Red Edge Biosignature Through Time on Earth and Exoplanets, Astrobiology, 18, 1123, doi: 10.1089/ast.2017.1798

Papageorgiou, G. C. 2004, in Chlorophyll a Fluorescence: A Signature of Photosynthesis, ed. G. C. Papageorgiou & Govindjee, Advances in Photosynthesis and Respiration (Dordrecht: Springer Netherlands), 43–63, doi: 10.1007/978-1-4020-3218-9_2

Porporato, A., D'Odorico, P., Laio, F., Ridolfi, L., & Rodriguez-Iturbe, I. 2002, Ecohydrology of water-controlled ecosystems, Advances in Water Resources, 25, 1335, doi: 10.1016/S0309-1708(02)00058-1

Porporato, A., D'Odorico, P., Laio, F., & Rodriguez-Iturbe, I. 2003, Hydrologic controls on soil carbon and nitrogen cycles. I. Modeling scheme, Advances in Water Resources, 26, 45, doi: 10.1016/S0309-1708(02)00094-5

Reinhard, C. T., Planavsky, N. J., Gill, B. C., et al. 2016, Evolution of the global phosphorus cycle, Nature, 541, 386, doi: 10.1038/nature20772

Ritchie, R. J., Larkum, A. W., & Ribas, I. 2017, Could photosynthesis function on Proxima Centauri b?, International Journal of Astrobiology, 17, 147, doi: 10.1017/S1473550417000167

Ross, R. T., & Calvin, M. 1967, Thermodynamics of Light Emission and Free-Energy Storage in Photosynthesis, Biophysical Journal, 7, 595, doi: 10.1016/S0006-3495(67)86609-8

Sagan, C., Thompson, W. R., Carlson, R., Gurnett, D., & Hord, C. 1993, A search for life on Earth from the Galileo spacecraft, Nature, 365, 715, doi: 10.1038/365715a0

Schwieterman, E. W., Kiang, N. Y., Parenteau, M. N., et al. 2018, Exoplanet Biosignatures: A Review of Remotely Detectable Signs of Life, Astrobiology, 18, 663, doi: 10.1089/ast.2017.1729

Seager, S., Turner, E., Schafer, J., & Ford, E. 2005, Vegetation's Red Edge: A Possible Spectroscopic Biosignature of Extraterrestrial Plants, Astrobiology, 5, 372, doi: 10.1089/ast.2005.5.372

Segura, A., Kasting, J. F., Meadows, V., et al. 2005, Biosignatures from Earth-Like Planets Around M Dwarfs, Astrobiology, 5, 706, doi: 10.1089/ast.2005.5.706

Segura, A., Krelove, K., Kasting, J. F., et al. 2003, Ozone Concentrations and Ultraviolet Fluxes on Earth-Like Planets Around Other Stars, Astrobiology, 3, 689, doi: 10.1089/153110703322736024

Stomp, M., Huisman, J., Stal, L. J., & Matthijs, H. C. P. 2007, Colorful niches of phototrophic microorganisms shaped by vibrations of the water molecule, The ISME Journal; London, 1, 271, doi: http://dx.doi.org/10.1038/ismej.2007.59

Takizawa, K., Minagawa, J., Tamura, M., Kusakabe, N., & Narita, N. 2017, Red-edge position of habitable exoplanets around M-dwarfs, Scientific Reports, 7, doi: 10.1038/s41598-017-07948-5

Tinetti, G., Rashby, S., & Yung, Y. L. 2006, Detectability of Red-Edge-shifted Vegetation on Terrestrial Planets Orbiting M Stars, The Astrophysical Journal, 644, L129, doi: 10.1086/505746

Tucker, C. J., & Maxwell, E. 1976, Sensor Design for Monitoring Vegetation Canopies, Photogrammetric Engineering, 42, 1399

Tyrrell, T. 1999, The relative influences of nitrogen and phosphorus on oceanic primary production, Nature, 400, 525, doi: 10.1038/22941

Wang, F., & He, J. 2021, Diurnal Variability and Detectability of Vegetation Red Edge of Earth-like Exoplanets, The Astrophysical Journal, 909, 9, doi: 10.3847/1538-4357/abd6ff

Wolstencroft, R., & Raven, J. 2002, Photosynthesis: Likelihood of Occurrence and Possibility of Detection on Earth-like Planets, Icarus, 157, 535, doi: 10.1006/icar.2002.6854